This is the published version of:

When citing this work, cite the original published paper.

IAC–17–A6.2.6

Evolution of Fragmentation Cloud in Highly Eccentric Orbit using Representative Objects

Stefan Frey[a*], Camilla Colombo[a], Stijn Lemmens[b], Holger Krag[b]

[a]*Politecnico di Milano, Department of Aerospace Science and Technology, Milan, Italy*
[b]*Space Debris Office, ESOC/ESA, Darmstadt, Germany*
[*]*Corresponding author; stefan.frey@polimi.it*

Abstract

Many historical on-orbit satellite fragmentations occurred in Highly Eccentric Orbits (HEOs) such as the Geostationary Transfer Orbit (GTO). Such fragmentations produce fragment clouds that interfere with the Low Earth Orbit (LEO) environment and pose a threat to operational satellites. Objects in HEO undergo complex dynamics due to the influence of perturbations varying as a function mainly of their altitude and area-to-mass ratio. The evolution of such a cloud, including small objects down to 1 mm, is not well understood.

This paper describes a method to model the evolution of a fragmentation cloud in HEO under the influence of atmospheric drag and Earth's oblateness. Semi-analytical techniques are applied to propagate representative objects constituting the cloud; rather than following the evolution of many distinct fragments. The proposed method is applied on a GTO upper stage using the standard NASA break-up model to find the distribution right after the fragmentation. The evolution of the fragment cloud is analysed statistically and time of closures are calculated for the formation of the torus along the parent orbit and the band around Earth. Assumptions on the evolution of the cloud that are valid in LEO are shown to be invalid for clouds in HEO.

Keywords: Fragment Cloud, Highly Eccentric, Representative Objects

1. Introduction

More than half of all the observable objects currently orbiting Earth originate from fragmentations of spacecraft or upper stages [1]. More fragments are being added every year. Since 1980, the 10-year average number of break-up events remains above 5 a year, some of them adding hundreds to thousands of new trackable objects [2]. Much effort was put into understanding the adverse consequences of such an on-orbit break-up towards collision probability of orbiting satellites [3] via deterministic or statistic methods that propagate the whole evolution of orbiting objects including fragments and operational spacecraft. Typically, the evolution of the cloud is separated into $3-4$ different phases [4, 5]:

1. Shortly after the break-up, the cloud forms an **ellipsoid** due to different velocity conditions of the fragments relative to the main body;

2. Owing to different semi-major axes and their corresponding periods, it quickly evolves into a **torus**, spreading the fragments along the orbit;

3. Being differently susceptible to precession rates mainly induced by Earth's oblateness, the fragments spread in right ascension and argument of perigee;

4. Finally, the cloud forms a **band** around Earth that extends in values of latitude approximately up to the inclination of the parent orbit.

Ideally, the perturbations acting on the evolution of the cloud can be separated by the phases, e.g. forces induced by drag are only considered after the formation of the band [5, 6]. For near-circular orbits in Low Earth Orbit (LEO), this assumption is generally valid as the time for the band to form (couple of months to years) is usually small compared to the rate of decrease in altitude. The dynamics in the last phase can then be studied analytically, incorporating also small objects and taking into account a simplified air drag model [7, 8, 9]. However, for objects in highly eccentric orbit (HEO), especially with low perigee heights, this assumption does not always hold true. The time it takes to form the band can span several decades.

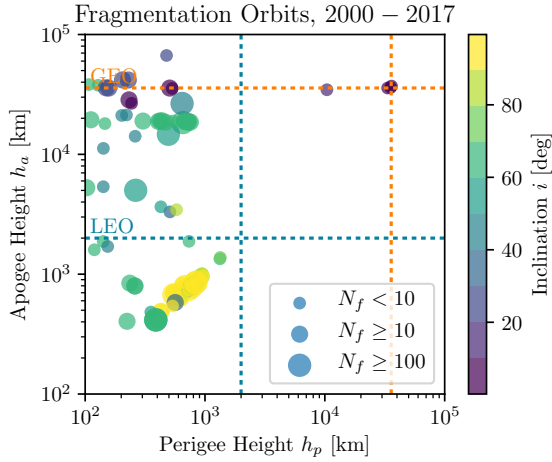Since 2000, 42 out of the 90 non-deliberate, on-

Fig. 1: On-orbit fragmentations since the year 2000, excluding collisions and deliberate explosions. The area and colour of the points describe the number of resulting observable fragments, N_f, and the inclination respectively.

orbit explosions occurred in HEO (see Figure 1), resulting on average in 26.9 observable objects across a large inclination range [1]. However, the available literature on the evolution of fragment clouds in HEO is sparse. Jenkin and Sorge [10] studied only the short-term behaviour and impact of debris clouds from an isotropic break-up in eccentric orbit in unperturbed, Keplerian motion. Letizia et al. [11] extended the continuity equation method to incorporate eccentricity, however the method is limited to low eccentric orbits ($e < 0.1$). Tools to predict the future space debris environment like LEGEND [12] and DELTA [13], can incorporate fragmentations in any orbit. But they are based on drawing discrete fragments from a given break-up probability distribution, getting statistical relevance only via many Monte Carlo runs. This gives little insight into the ramifications of a single break-up in HEO.

In this paper, the evolution of the debris cloud originating from a fragmentation in the Geostationary Transfer Orbit (GTO) is studied. GTO is a subset of HEO containing more than 200 large upper stages that delivered spacecraft into the Geostationary Orbit (GEO), and now cross the highly populated LEO region at velocities larger than 11 km/s. Collision probabilities in GTO are small [14], but each new fragmentation will add objects that potentially lead to follow-up collisions with LEO residents.

Starting from the NASA break-up model [15], a

method is presented to select representative fragments. These fragments are propagated under the influence of air-drag and the second order zonal harmonic, J_2. The assumption of separating the evolution of the cloud into different phases is tested with a simulated upper stage explosion in GTO, by studying the distribution of the fragment orbital elements.

The paper is organised as follows: the methodology is described in Section 2 to 5. Section 2 describes the fragmentation model, Section 3 the selection of the representative objects via gridding, Section 4 the applied propagation scheme and Section 5 the derivation of decay rate and time of closure. Section 6 shows results for a simulated fragmentation and Section 7 summarises the conclusion reached and proposes future work.

2. Fragmentation Model

The key indicators of a fragment cloud are number of fragments, N_f, generated via an explosion or collision event in space, and the area-to-mass ratio, A/m, and relative velocity with respect to the parent orbit, $\Delta \boldsymbol{v}$, of each resulting fragment. The NASA break-up model [15] provides N_f as a function of the characteristic length, L_c, and the probability distributions for A/m and relative velocity magnitude $\Delta v = ||\Delta \boldsymbol{v}||$, conditionally dependent on L_c and A/m respectively. The probability density functions (PDFs) of these variables are given below. The direction of the relative velocity, $\boldsymbol{n}_{\Delta v} = \frac{\Delta \boldsymbol{v}}{\Delta v}$, is assumed to be isotropic.

2.1 Characteristic Length L_c

The number of fragments are defined differently for explosions and collisions and subsequently described.

2.1.1 Explosions

The cumulative number of fragments for an explosions is [15]

$$N^E(L_c) = 6SL_c^{-1.6} \tag{1}$$

where S is a type-dependent, unitless number. From Equation 1, and introducing the cut-off characteristic length $L_{c,\theta} = 1$ mm, the cumulative distribution function (CDF) $F_{L_c}^E$ can be found as

$$F_{L_c}^E(L_c, L_{c,\theta}) = \begin{cases} 1 - \left(\dfrac{L_c}{L_{c,\theta}}\right)^{-1.6} & \forall L_c > L_{c,\theta} \\ 0 & \text{otherwise} \end{cases} \tag{2}$$

and by taking its derivative, the PDF $f_{L_c}^E$ is

$$f_{L_c}^E(L_c, L_{c,\theta}) = \begin{cases} 1.6 \dfrac{L_c^{-2.6}}{L_{c,\theta}^{-1.6}} & \forall L_c > L_{c,\theta} \\ \\ 0 & \text{otherwise} \end{cases} \quad (3)$$

2.1.2 Collisions

Similarly, the cumulative number of fragments for a collision can be approximated as [15]

$$N^C(L_c) = 0.1 M^{0.75} L_c^{-1.71} \quad (4)$$

where $M = M(M_t, M_p, \Delta v_r, \theta)$ is the mass involved in the fragmentation and dependent on the collision energy. It can be derived from the target and projectile masses, M_t and M_p, the relative collision velocity between the target and the projectile, Δv_r, and the threshold specific kinetic energy, θ, typically set as $\theta = 40$ kJ/kg [16].

Again, the derivations of the CDF and PDF are straightforward

$$F_{L_c}^C(L_c, L_{c,\theta}) = \begin{cases} 1 - \left(\dfrac{L_c}{L_{c,\theta}}\right)^{-1.71} & \forall L_c > L_{c,\theta} \\ \\ 0 & \text{otherwise} \end{cases} \quad (5)$$

$$f_{L_c}^C(L_c, L_{c,\theta}) = \begin{cases} 1.71 \dfrac{L_c^{-2.71}}{L_{c,\theta}^{-1.71}} & \forall L_c > L_{c,\theta} \\ \\ 0 & \text{otherwise} \end{cases} \quad (6)$$

2.2 Area-to-Mass Ratios A/m

The PDF of A/m, is defined in the logarithmic space with base 10, and conditionally dependent on $\lambda_c = \log_{10} L_c$. With $\chi = \log_{10}(A/m)$, it is defined as a weighted summation of normal distributions $\mathcal{N}(\cdot, \mu, \sigma)$

$$f_{\frac{A}{m}|L_c}(\chi, \lambda_c) = \sum_{i=1}^{3} \beta_i \alpha_i \mathcal{N}(\chi, \mu_i, \sigma_i|\lambda_c) \quad (7)$$

where α_i, μ_i and σ_i are a function of the dependent variable λ_c and different for fragmenting spacecraft or upper stages. The parameters for small ($L_c < L_c^s = 8$ cm; $i = 1$) and large ($L_c > L_c^l = 11$ cm; $i = 2, 3$) fragments for both types can be found in [15]. Here, a bridging function, $\beta_i = \beta_i(\lambda_c)$, is introduced that ensures continuous transition between $L_c^s < L_c < L_c^l$. Both the parameters for small and large fragments are continued into the transition phase and weighted linearly

$$\beta_i(\lambda_c) = \begin{cases} \beta(\lambda_c) & \text{for } i = 1 \\ 1 - \beta(\lambda_c) & \text{for } i = 2, 3 \end{cases} \quad (8)$$

where (defining $\lambda_c^s = \log_{10} L_c^s$ and $\lambda_c^l = \log_{10} L_c^l$)

$$\beta(\lambda_c) = \begin{cases} 1 & \forall \lambda_c < \lambda_c^s \\ 0 & \forall \lambda_c > \lambda_c^l \\ 1 - \dfrac{\lambda_c - \lambda_c^s}{\lambda_c^l - \lambda_c^s} & \text{otherwise} \end{cases} \quad (9)$$

Figure 2a shows the PDF in A/m for different L_c and A/m for the case of an upperstage fragmentation. The dashed lines highlight the bridging function between small and large fragments. Most of the explosion fragments have an A/m within $0.1 - 2$ m^2/kg.

2.3 Relative Velocity Magnitudes Δv

The probability of relative velocity between the parent orbit and the fragments, Δv, is described via a single normal distribution in the $\log_{10}$-space, with A/m as the conditional dependent variable. The parameters defining the distributions are different for spacecraft and upper stages. The values can be found in [15]. Defining $\nu = \log_{10}(\Delta v)$, the PDF is

$$f_{\Delta v|\frac{A}{m}}(\nu, \chi) = \mathcal{N}(\nu, \mu_\nu, \sigma_\nu|\chi) \quad (10)$$

Figure 2b shows the PDF in Δv in case of an explosion.

3. Selection of Representative Fragments

The PDF of a single object having characteristics L_c, A/m and Δv can be found by combining Equations 3 or 5 with 7 and 10

$$f_{L_c, \frac{A}{m}, \Delta v} = f_{\Delta v|\frac{A}{m}} f_{\frac{A}{m}|L_c} f_{L_c} \quad (11)$$

The number of dimensions can be reduced by reduction of L_c, which is not a relevant parameter for the propagation

$$f_{\frac{A}{m}, \Delta v} = f_{\Delta v|\frac{A}{m}} \int_{L_c} f_{\frac{A}{m}|L_c} f_{L_c} dL_c \quad (12)$$

To find the evolution of the cloud, three different approaches can be taken:

- Draw and propagate distinct fragments. However, this requires many instances and the outcome will be different for every run;

- Convert the distribution into convenient elements to propagate directly the density of fragments. However, this requires a closed-form solution that is accurate enough for the conversion of the PDF;
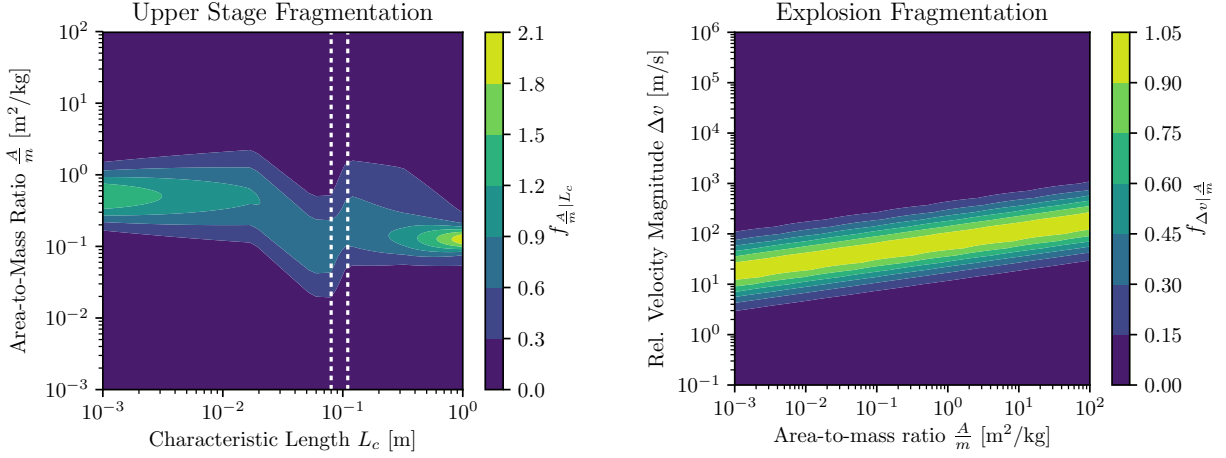
(a) Probability distribution in A/m for a single fragment given L_c and A/m. The dashed lines mark the bridged region.

(b) Probability distribution in Δv for a single fragment with given A/m and Δv.

Fig. 2: Fragment distribution for an upper stage explosion.

- Find representative objects that describe the cloud accurately and completely enough in terms of probabilities.

The second approach can be implemented via the Gauss planetary equations [17]. Yet these equations were conceived assuming small accelerating perturbations. According to the model described in Section 2, around 30% of the fragments have a $\Delta v > 100$ m/s. For such a Δv, the Gauss planetary equations start to divert from the solution obtained by converting a parent orbit from Keplerian elements into Cartesian coordinates, adding the perturbation and converting back (see Figure 3).

Instead, the approach of selecting representative objects is applied.

In order to find representative objects, the remaining two dimensions, A/m and Δv, are split into N_i and N_j finite, logarithmically spaced bins, $d(A/m)_i$ and $d(\Delta v)_j$, each two-dimensional bin representing an object having the characteristics $A/m \in d(A/m)_i$ and $\Delta v \in d(\Delta v)_j$, with the probability

$$P^{ij}_{\frac{A}{m},\Delta v} = \int_{\frac{A}{m}} \int_{\Delta v} f_{\frac{A}{m},\Delta v} d(\Delta v)_j d(A/m)_i \qquad (13)$$

Instead of logarithmic bins, the bin sizes could also be chosen such that all representative objects are equally likely, which was shown to be more accurate [8]. However, the selection of equally likely objects over a complex two-dimensional probability distribution is outside of the scope of this paper.

To reduce the number of propagations, the grid points with probability less than the α-quantile, q_α, over all (ij), are discarded. Figure 4a shows the grid for an upper stage explosion, for $N_i = N_j = 100$ and $\alpha = 99.9\%$.

To fully describe a fragment, the probability and thus the grid in $\boldsymbol{n}_{\Delta v}$ needs to be defined. Here, a Fibonacci lattice [18] was used to define the two direction angles, the longitude, θ and the latitude, ϕ. The Cartesian coordinates in which $\boldsymbol{n}_{\Delta v}$ is defined can be chosen arbitrarily, as the distribution is isotropic and thus invariant under coordinate transformations. Each of the N_k direction grid points, quasi-uniformly distributed over the sphere, are assumed to be equally likely with $P_{\boldsymbol{n}_{\Delta v}} = \frac{1}{N_k}$. An example showing a Fibonacci lattice with $N_k = 101$ points can be found in Figure 4b.

Hence, the final grid point probability is

$$P^{ijk}_{\frac{A}{m},\Delta v,\boldsymbol{n}_{\Delta v}} = \frac{1}{N_k} P^{ij}_{\frac{A}{m},\Delta v} \qquad (14)$$

Note that the theory is developed looking only at a single fragment and its probability of presence in the characteristics A/m and $\Delta \boldsymbol{v}$, comparable to the quantum state describing the electron PDF around atom nuclei in quantum mechanics. However, by multiplying Equation 14 with the (constant) number of fragments N_f, and assuming no inter-fragment interaction, the distribution of the whole cloud can be deduced. Hence, the distribution of the fragment and
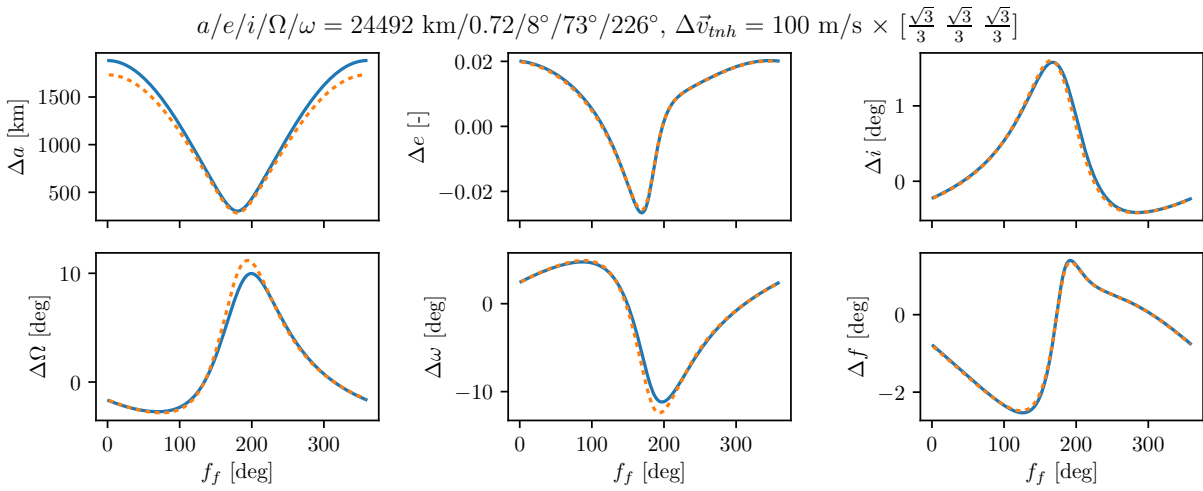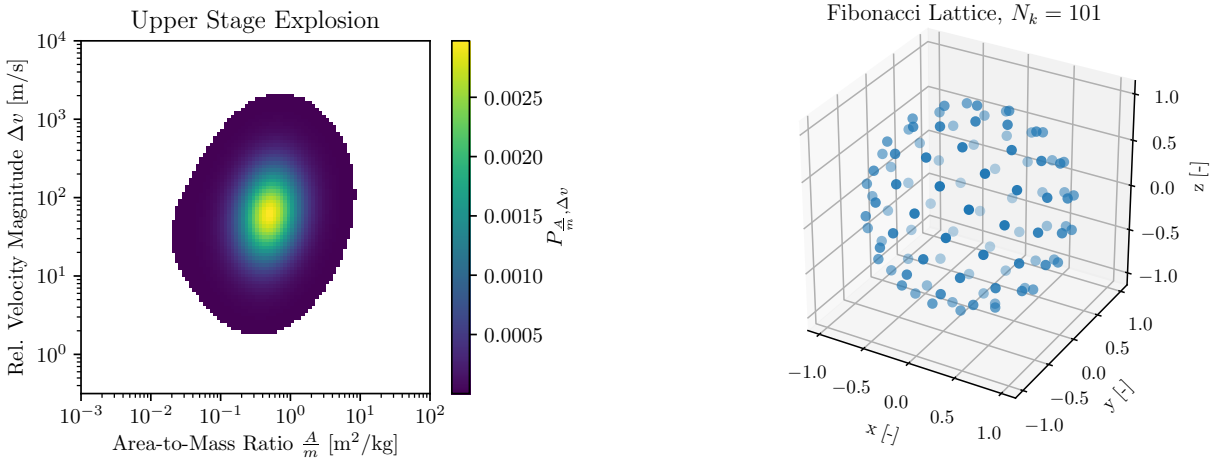
$a/e/i/\Omega/\omega = 24492$ km$/0.72/8°/73°/226°$, $\Delta\vec{v}_{tnh} = 100$ m/s $\times [\frac{\sqrt{3}}{3} \frac{\sqrt{3}}{3} \frac{\sqrt{3}}{3}]$

Fig. 3: Comparison of perturbing an orbit with $\Delta v = 100$ m/s by using direct transformations (solid line) and Gauss planetary equations (dotted).

(a) Grid with 100 bins in each direction over $P_{\frac{A}{m},\Delta v}$ along A/m and Δv for an upper stage explosion, resulting in 2635 representative objects, representing 99.9% of all objects.

(b) Grid over θ and ϕ, each point with quasi-equal probability.

Fig. 4: Selection of representative objects via grid in the dimensions critical for propagation.

Table 1: Smooth atmosphere density model parameters, resulting from a fit to Jacchia-77 [22], with an exospheric temperature, $T_\infty = 750$ K.

p	H_p [km]	$\rho_{0,p}$ [kg/m^3]
1	4.880	$3.932 \times 10^{+02}$
2	9.734	2.099×10^{-03}
3	20.25	1.462×10^{-06}
4	33.54	2.386×10^{-08}
5	47.52	2.808×10^{-09}
6	136.1	2.384×10^{-13}
7	239.1	5.070×10^{-14}
8	1073	5.988×10^{-16}

the distribution of the fragment cloud is used interchangeably throughout this report.

4. Orbit Propagation

Since many grid points have to be propagated for a long time, the semi-analytical propagator PlanO-Dyn [19] is used. The fragment cloud is subjected to the second-order zonal harmonic, J_2, and air-drag. Solar radiation pressure and luni-solar effects are neglected in this work and will be added in a future extension. Owing to differences in the initial conditions, the effect of J_2 leads to different precession speeds in ascending node, Ω, and argument of perigee, ω, ultimately leading to the fragment cloud being spread into a band around Earth. The air-drag removes energy from each fragment, forcing it to decay. Here, a smooth exponential atmosphere density model, ρ_S, combined with the superimposed King-Hele contraction model is used to calculate the rate of orbit decay [20, 21]. The model, dependent on the altitude, h, and valid for any $h > 100$ km is defined as

$$\rho_S(h) = \sum_{p=1}^{P} \rho_{0,p} \exp{-\frac{h}{H_p}} \qquad (15)$$

with base densities, $\rho_{0,p}$, and scale heights, H_p, listed in Table 1.

The fragment initial conditions and characteristics depend on the parent orbit and location, $\boldsymbol{\alpha}_p = (a, e, i, \Omega, \omega, f)$, and the grid given in Section 3, with the semi-major axis, a, eccentricity, e, inclination, i, and true anomaly, f. As $\boldsymbol{n}_{\Delta v}$ is given in (any) Cartesian coordinates, $\boldsymbol{\alpha}_p$ needs to be transformed into the same coordinates, $\boldsymbol{r}_p = (\boldsymbol{x}, \boldsymbol{v})$, before applying the velocity variation. Subsequently, the deviated coordinates, $\boldsymbol{r}_{jk} = (\boldsymbol{x}, \boldsymbol{v} + \Delta \boldsymbol{v}_{jk})$, are transformed back into Keplerian elements, $\boldsymbol{\alpha}_{jk}$, for propagation. Note that

Table 2: Fragmentation parent orbit in GTO and fragmenting at perigee.

a [km]	e	i [deg]	Ω [deg]	ω [deg]	f [deg]
24492	0.7188	8.4	73.4	225.9	0

the deviated initial conditions use the mean anomaly, M, as a starting point of each propagation.

The representative objects are propagated for 200 years or up until re-entry.

5. Decay Rate and Time of Closure

Given the propagated cloud, the probability of an fragment to be within a certain phase space, $P_f(\Delta t)$, at a given time after the fragmentation, Δt, is estimated by summing up the grid probabilities, $P^{ijk}_{\frac{A}{m}, \Delta v, \boldsymbol{n}_{\Delta v}}$, of all the propagated initial conditions that reside in that space at time Δt. Summing up all P_f over the whole physically valid phase space results in the on-orbit dwelling probability, P_d.

To calculate the time of closure, T, a Kuiper's test [23] is performed, comparing the distribution against the uniform hypothesis on a circle, H_0: $f_{H_0}(x) = \frac{1}{2\pi} \; \forall x \in [0, 2\pi]$. This test is ideal for distributions on a circle, as the result is independent from the starting value for the calculation of the CDF. H_0 is rejected as long as the p-value, p, is lower than $\alpha_p = 5\%$. Since the PDF is not sampled, but gridded over, the effective number of samples, N_e, to calculate p cannot be chosen as N. Instead, an optimistic $N_e^{-1} = \max_{ijk} P^{ijk}$ is chosen. Such a test is performed for the distributions in Ω, ω and M, resulting in T_Ω, T_ω and T_M. The formation of the band around Earth is reached, when $\Delta t = T_B = \max(T_\Omega, T_\omega, T_M)$.

To give a measure of the influence of air-drag on the evolution of the cloud, the a- and e-quantiles, q_α, are calculated, giving the evolution of the upper limit in a and e of α percent of all the object probability.

6. Results

A upper stage explosion is simulated in GTO, following a real event in January 2001 of the fragmentation of a then 12 year old Ariane 2 third stage [24]. As the fragmentation location is unknown, it is arbitrarily chosen to be at $f = 0°$. Table 2 contains the parent orbit information. All fragments with length between $10^{-3} \leq L_c \leq 10^1$ m are considered. The grid in A/m and Δv is done in $N_i = N_j = 100$ logarithmic steps from $10^{-3} \leq \frac{A}{m} \leq 10^2$ m^2/kg and $10^{-1} \leq \Delta v \leq 10^4$ m/s respectively. Only
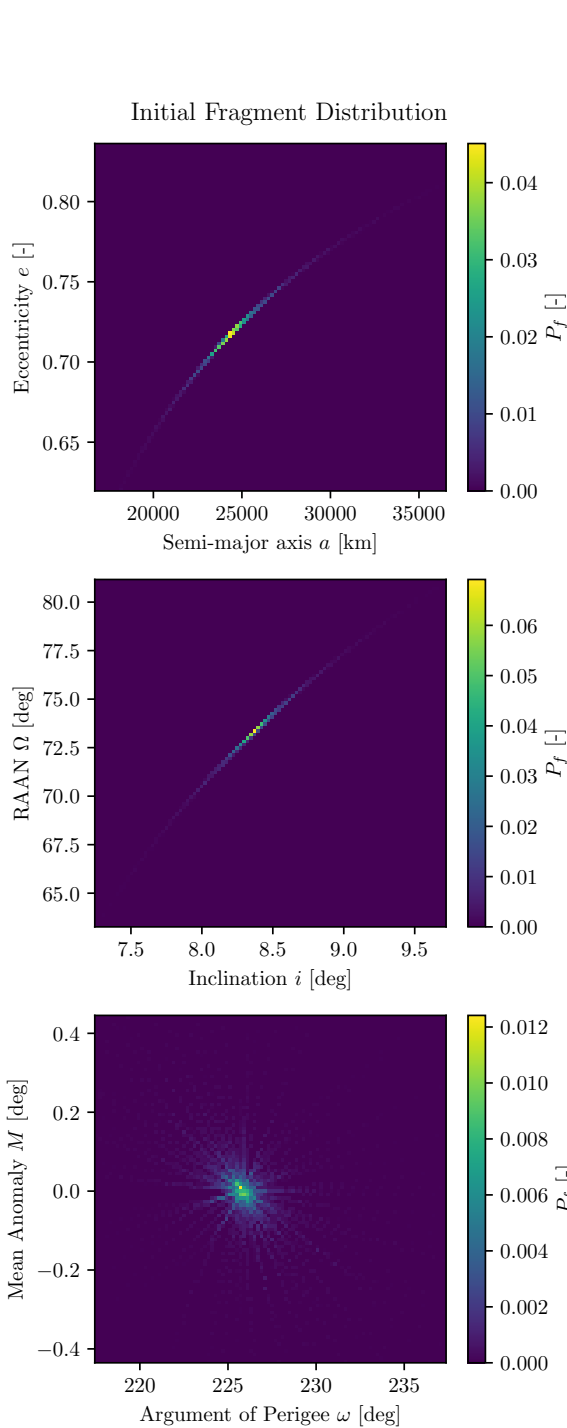
Initial Fragment Distribution

Decay Rate

Fig. 6: Probability of a fragment still dwelling on-orbit after Δt. A near linear decay rate of 1.25% per decade can be observed.

the grid points with $P^{ij}_{\frac{A}{m},\Delta v} > q_{99.9\%}$ are considered and N_k was chosen to be 101, leading to a total of $N = 266135$ initial points to be propagated. Figure 5 shows the probability distribution of a fragment right after the fragmentation. The distribution in M is very confined for a fragmentation at perigee.

The probability of a single fragment, stemming from the given upper stage explosion and larger than $L_c > 10^{-3}$ m to still dwell on-orbit after Δt is given in Figure 6. The initial decrease of about 2% right after the fragmentation is due to fragment characteristics leading to perigee heights within Earth's radius, and thus are removed instantaneously from the propagation. The oscillating behaviour is caused by multiple representative fragments with the same A/m, re-entering as clusters, a result from the grid being to coarse. A near constant decrease of 1.25% per every 10 years can be observed. The very slow re-entry rates are due to the conservative atmosphere model chosen, simulating a solar minimum for the next 200 years.

The evolution in Ω, ω and M can be found in Figure 7. Clearly recognisable is the precession of all the variables with J_2, superimposed with the spreading due to different initial conditions. As expected, the fast moving variable M reaches closure first, after less than 1 year. The time needed for the randomisation in Ω and ω is similar in order of magnitude; $T_\Omega = 65$ years and $T_\omega = 41$ years respectively. Finally, the band is formed after $T_B = 65$ years.

Figure 8 shows the evolution of the PDF in a

Fig. 5: Initial fragment distribution right after the upper stage explosion at perigee. See Table 2 for the definition of the parent orbit.

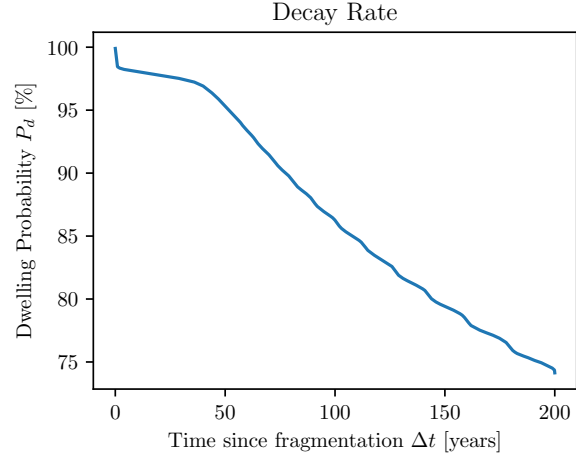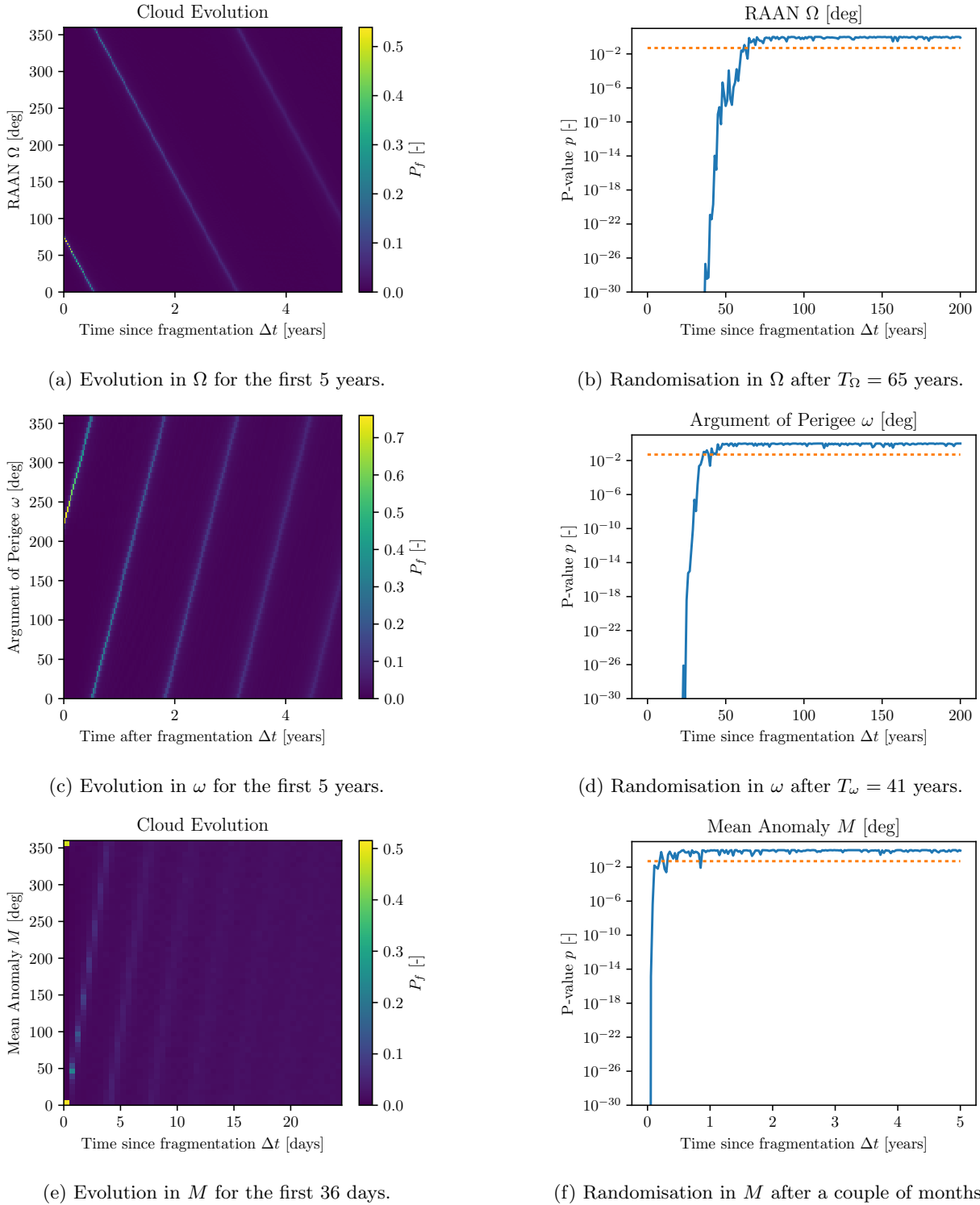(a) Evolution in Ω for the first 5 years.

(b) Randomisation in Ω after $T_\Omega = 65$ years.

(c) Evolution in ω for the first 5 years.

(d) Randomisation in ω after $T_\omega = 41$ years.

(e) Evolution in M for the first 36 days.

(f) Randomisation in M after a couple of months.

Fig. 7: Evolution of distribution of Ω, ω and M. Left: probability distribution, right: Kuiper's statistic (dashed line: $\alpha_p = 5\%$). Note the differences in ranges for Δt.
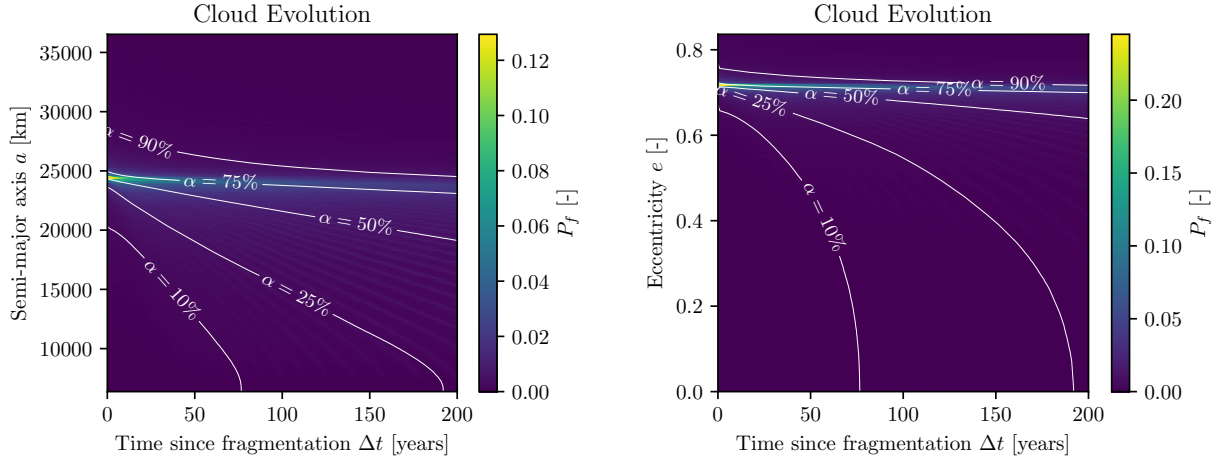
(a) The peak density remains almost constant in location, while becoming smaller due to spreading towards lower a.

(b) Likewise, the peak probability remains close to the initial peak, while spreading towards smaller e.

Fig. 8: Evolution of distribution in a and e for 200 years. The colormap shows the probability in presence, while the quantiles, q_α, divide the lower α and the upper $1 - \alpha$ percent of the presence probability.

Table 3: Evolution of fragment distribution for different grid sizes; time required for 25% of the fragment probability to decay ($q_{25\%}$) and upper limit in a for 50% ($q_{50\%}$), and 75% ($q_{75\%}$) of the distribution after 200 years.

N_i	N_j	N_k	$q_{25\%}$ [years]	$q_{50\%}$ [km]	$q_{75\%}$ [km]
25	25	25	169.9	18809	23079
50	50	50	187.9	18995	23150
75	75	75	192.9	19260	23215
100	100	101	193.9	19275	23248
50	100	101	190.9	19203	23257
100	50	101	195.9	19399	23232
100	100	51	196.9	19413	23213

and e together with the q_α overlayed. 65 years after the fragmentation, the a-band containing 50% of the probability distribution from $q_{25\%}$ to $q_{75\%}$ almost quintuples from 1300 to more than 6000 km. The equivalent e-band increases more than 6-fold in the same time range (from 0.015 to 0.099). At the same time, the peak density in a shifts by -360 km and shrinks by 70% after 65 years. The peak density in e shifts by -0.004 and also shrinks by the same amount. The alert reader can spot *rays* in the figures, again representing clusters of representative objects with the same A/m. The lower N_i is chosen, the less – but instead more pronounced – the *rays* could be

discerned. Interpolation between the grid points, i.e. using differential algebra, would remove these remnants of the grid. For qualitative description of the cloud, the size of the grid points for this orbit can be chosen lower, as the evolution profile saturates after $N_i \times N_j \times N_k = 50 \times 50 \times 51$ (see Table 3).

The shape of the PDF in a and e changes considerably during the formation of the band. Thus it is not valid to ignore air-drag during this time. It is still to be checked if the evolution of the real fragmentation cloud follows the one calculated here. Unfortunately, as only large fragments are observed (less than 100), the comparison would yield only little insight.

7. Conclusion and Future Work

Traditionally, the evolution of a cloud of fragments in LEO is separated by phases. The time to form a torus along the parent orbit is short enough to ignore perturbations. Then, while the cloud spreads out to form a band due to J_2, the influence of air-drag is neglected. Lastly, after the formation of the band, only air-drag is considered. For each of these phases, the evolution of the fragment distribution is described [5, 8].

This paper showed on a study case in GTO using the NASA break-up model [15] and representative fragments propagated semi-analytically, that the time for formation of the torus along the parent orbit requires months and the formation of the band around Earth requires 10s of years in HEO. Enough

time passes, for the evolution in a and e to change considerably, making the assumption that air-drag plays a minor role until formation of the band invalid.

Future work includes the addition of solar radiation pressure and third body perturbations during propagation, the study of different parent orbit configurations, the removal of sensitivity on the selection of grid points via differential algebra and the calculation of the collision risk for objects in LEO following a fragmentation in HEO. Further, instead of propagating representative fragments, the probability density function will be calculated directly in Keplerian elements to allow for a density based propagation of the cloud.

Acknowledgement

References

[1] T. Flohrer, S. Lemmens, B. Bastida Virgili, H. Krag, H. Klinkrad, N. Sanchez, J. Oliveira, and F. Pina. DISCOS - current status and future developments. In *Proceedings of the 6th European Conference on Space Debris*, 2013. `https://discosweb.esoc.esa.int`.

[2] V. Braun, S. Lemmens, B. Reihs, H. Krag, and A. Horstmann. Analysis of breakup events. In *Proceedings of the 7th European Conference on Space Debris*, 2017.

[3] S. P. Barrows, G. G. Swinerd, and R. Crowther. Review of debris-cloud modeling techniques. *Journal of Spacecraft and Rockets*, 33(4):550–555, 1996.

[4] D. McKnight and G. Lorenzen. Collision matrix for low earth orbit satellites. *Journal of Spacecraft*, 26(2):90–94, 1989.

[5] R. Jehn. Dispersion of debris clouds from on-orbit fragmentation events. In *41st Congress of the International Astronautical Federation*, 2009.

[6] J. Ashenberg. Formulas for the phase characteristics in the problem of low earth orbital debris. *Journal of Spacecraft and Rockets*, 31(6):1044–1049, 1994.

[7] C. R. McInnes. Compact analytic solutions for a decaying, precessing circular orbit. *The Aeronautical Journal*, 98(979):357–360, 1994.

[8] F. Letizia, C. Colombo, and H. G. Lewis. Analytical model for the propagation of small-debris-object clouds after fragmentations. *Journal of Guidance, Control and Dynamics*, 38(8):1478–1491, 2015.

[9] Z. Binbin, W. Zhaokui, and Z. Yulin. An analytic method of space debris cloud evolution and its collision evaluation for constellation satellites. *Advances in Space Research*, 58(6):903–913, 2016.

[10] A. B. Jenkin and M. E. Sorge. Debris clouds in eccentric orbits. In *AIAA Space Programs and Technologies Conference*, 1990.

[11] F. Letizia, C. Colombo, and H. G. Lewis. Multi-dimensional extension of the continuity equation method for debris clouds evolution. *Advances in Space Research*, 57(8):1624–1640, 2016.

[12] J.-C. Liou, D. T. Hall, P. H. Krisko, and J. N. Opiela. LEGEND - a three-dimensional LEO-to-GEO debris evolutionary model. *Advances in Space Research*, 34(5):981–986, 2004.

[13] B. Bastida Virgili. DELTA debris environment long-term analysis. In *6th International Conference on Astrodynamics Tools and Techniques*, 2016.

[14] S. Frey and S. Lemmens. Status of the space environment: Current level of adherence to the space debris mitigation policy. *Journal of the British Interplanetary Society*, 70(02-04):118–124, 2017.

[15] N. L. Johnson, P. H. Krisko, J.-C. Liou, and P. D. Anz-Maedor. NASA's new breakup model of EVOLVE 4.0. *Advances in Space Research*, 28(9):1377–1384, 2001.

[16] P. H. Krisko. Proper implementation of the 1998 NASA breakup model. *Orbital Debris Quarterly News*, 15(4):4–5, 2011.

[17] R. H. Battin. *An Introduction to the Mathematics and Methods of Astrodynamics, Revised Edition*. AIAA, 1999.

[18] R. Swinbank and R. J. Purser. Fibonacci grids: A novel approach to global modelling. *Quarterly Journal of the Royal Meteorological Society*, 132(619):1769–1793, 2006.

[19] C. Colombo. Long-term evolution of highly-elliptical orbits: luni-solar perturbation effects for stability and re-entry. In *25th AAS/AIAA Space Flight Mechanics Meeting*, 2015.

[20] S. Frey and C. Colombo. Superimposition of the atmosphere density for fast and accurate semi-analytical propagation. In *KePASSA 2017: International Workshop on Key Topics in Orbit Propagation Applied to Space Situational Awareness*, 2017.

[21] D. King-Hele. *Theory of satellite orbits in an atmosphere*. London Butterworths, 1964.

[22] L. G. Jacchia. Thermospheric temperature, density, and composition: new models. *SAO Special Report 375*, 1977.

[23] N. H. Kuiper. Tests concerning random points on a circle. In *Indagationes Mathematicae Proceedings*, 1960.

[24] NASA's Orbital Debris Program Office. History of on-orbit satelllite fragmentations, 14th edition, 2008.